JOURNAL OF MATERIALS SCIENCE 28 (1993) 2245–2259

Microstructural evolution and mechanical properties of SiC/Al_2O_3 particulate-reinforced spray-deposited metal-matrix composites

M. GUPTA, F. MOHAMED, E. LAVERNIA
Materials Science and Engineering, Department of Mechanical and Aerospace Engineering, University of California, Irvine, CA 92717, USA

T.S. SRIVATSAN
Department of Mechanical Engineering, The University of Akron, Akron, Ohio 44325, USA

In this study, aluminium–copper-based metal-matrix composites were synthesized utilizing the spray atomization and co-deposition technique. Microstructural characterization studies were carried out with an emphasis on understanding the effects associated with the co-injection of silicon carbide and aluminium oxide particulates. The results demonstrate the ageing kinetics of the spray-deposited and hot-extruded metal-matrix composites to be the same as those of the monolithic aluminium–copper material. Results of ambient temperature mechanical tests demonstrate that the presence of particulate reinforcement in the metal matrix does little to improve strength, and degrades the ductility of the matrix material. A model is formulated to compute the critical volume fraction of reinforcement. The results obtained using this model suggest that an optimum volume fraction of silicon carbide is essential in order to realize a strength improvement in the metal-matrix composite, relative to their monolithic counterpart.

1. Introduction

Discontinuously reinforced aluminium (DRA) composites have over the years been the subject of intensive study due to their innate ability to combine superior strength, high stiffness, low density and fracture resistance [1]. Commonly utilized matrix materials include aluminium alloys based on the 2XXX (Al–Cu), 6XXX (Al–Mg–Si) and more recently the 7XXX (Al–Zn–Mg–Cu) series. The discontinuous reinforcements include particulates, chopped fibres and whiskers. The primary advantage of using discontinuous reinforcements is that the metal-matrix composites are relatively easy to fabricate by both powder metallurgy (PM) and ingot metallurgy (IM) techniques and the resulting products exhibit near-isotropic behaviour. Commonly used reinforcements for aluminium alloy matrices include silicon carbide (SiC) and aluminium oxide (Al_2O_3).

In recent studies, investigators have succeeded in tailoring the properties of existing aluminium alloys to specific applications through compositional modifications. One such example is alloy AA 2519 (Al–Cu–Mg), which has demonstrated excellent strength and ballistic performance coupled with good stress corrosion cracking resistance [2]. In an effort to achieve additional improvements in the properties of alloys such as AA 2519, a variety of synthesis techniques are actively being studied. One such technique is spray atomization and deposition which has received considerable attention for the synthesis of aluminium-base alloys [3–5] and metal-matrix composites (MMCs) [6–14]. This novel technique involves processing in a regime of the phase diagram where the alloy is a mixture of solid and liquid phases. Such an approach would inherently avoid the extreme thermal excursions with concomitant degradation in interfacial properties and extensive macrosegregation normally associated with conventional casting processes [15, 16]. Furthermore, this approach also eliminates the need to handle fine reactive particulates, as is necessary with powder metallurgical (PM) processes [17, 18].

The objective of the present study was to provide an insight into the effects of co-injection of SiC and Al_2O_3 particulates during spray atomization and co-deposition processing, henceforth referred to as spray processing, on the microstructure and mechanical behaviour of aluminium alloy AA 2519. The effects of SiC and Al_2O_3 particulates on the microstructure during solid-state cooling, that is after the matrix–particulate mixture has arrived on the substrate, were investigated with particular emphasis on the rate of grain growth. To identify the role of particulate reinforcement on grain boundary migration, the reinforced matrix and unreinforced material were exposed to various isothermal heat treatments. The intrinsic microstructural features of the spray-processed metal-matrix composite are characterized and discussed in the light of alloy composition and processing variables. The ambient-temperature mechanical properties of the composite are correlated with microstructural features.

0022–2461

2. Experimental procedure

2.1. Processing

The experimental studies were conducted on an Al–(5.0–7.0)Cu–(0.1–0.3)Mg–(0.0–0.8)Mn–(0.0–0.1)Ti–(0.0–0.25)V–(0.0–0.25)Zr–(0.0–0.5)Fe–(0.0–0.5)Si–(0.0–0.12)Zn (wt %) (designated as alloy AA 2519) alloy. The alloy was provided, in the form of rolled plates, by the Army Materials Technology Laboratory (AMTL: Watertown, Massachusetts, USA). The matrix alloy will be henceforth referred to as Al–Cu. The size distributions of the SiC (α phase) and Al_2O_3 (α phase) particulates were Gaussian and exhibited an average size of 3 μm (d_{50}).

The MMCs were synthesized according to the following procedure. The Al–Cu matrix material was superheated to the temperature of interest (Table I), and disintegrated into a fine dispersion of micrometre-sized droplets using atomizing gas at a pre-selected pressure. Simultaneously, two jets each containing one type of ceramic particulate reinforcement (either SiC or Al_2O_3) and positioned at 180° with respect to each other were injected into the atomized matrix material at a previously selected flight distance. The flight distance was determined on the basis of a numerical analysis of the temperature and fraction of solid contained in the atomized matrix material. The reinforcement injection distance for experiments 3, 4 and 5 was 0.21 m, and the substrate position used was 0.41 m for all of the experiments. The selection of this injection distance was made on the basis of a study by Gupta *et al.* [19]. Their results showed that at a particular flight distance, the atomized aluminium alloy droplets have lost approximately 40–50% of their original enthalpy. Following co-injection, the mixture of rapidly quenched, partially solidified droplets with interdispersed ceramic particulates was deposited on a water-cooled deposition surface, eventually collecting as a coherent preform. The microstructure of the preform is dictated by the solidification conditions during impact. In order to avoid extensive oxidation of the aluminium alloy matrix during processing, the experiments were conducted in an environmental chamber. The latter was evacuated to a negative pressure of 0.020 MPa, and backfilled with inert gas to a positive pressure of 0.014 MPa, prior to melting and atomization. A schematic diagram of the experimental arrangement used in this study is shown in Fig. 1. A total of five experiments were conducted. The primary experimental variables used for each experiment are summarized in Table I.

The SiC and Al_2O_3 particulates were introduced into the atomized Al–Cu spray using an injector (Fig. 2). The injector consisted of a coaxial tube that entrained the ceramic particulates as the gas flowed from the inlet to the outlet orifices. The injection of the ceramic particulates was carried out at ambient temperature. A comprehensive discussion of the experimental details is provided elsewhere [6] and will not be reiterated here.

2.2. Microstructure

Microstructural characterization studies were conducted on both the unreinforced and reinforced matrix materials in order to determine: (a) the grain size, (b) volume fraction of SiC and Al_2O_3 particulates, and (c) the presence of secondary phases in the spray-atomized and deposited samples. In addition, density measurements were carried out on spray-deposited and extruded samples in order to ensure the closure of micrometre-sized porosity present in the as-spray deposited samples.

Optical microscopy was conducted on both polished and etched as-deposited samples using conventional and differential interference contrast (DIC) techniques. The use of DIC microscopy facilitated identification of the ceramic particulates in the matrix. The samples were sectioned to a thickness of 0.5 cm, polished using conventional techniques, and etched using Keller's reagent (0.5 HF–1.5 HCl–2.5 HNO_3 –95.5 H_2O). The grain size was measured using the linear intercept method, as described in ASTM E 112-84.

Density measurements were conducted on the polished, extruded samples utilizing the Archimedes principle. The weight of each sample was determined, using a Fisher Scientific A-250 Balance, to an accuracy of ± 0.0001 g. Ethylene glycol was used as the fluid.

The volume fraction of ceramic particulate (SiC or Al_2O_3) was determined using a chemical dissolution method. This method involved: (i) measuring the mass of composite samples, (ii) dissolving the samples in dilute hydrochloric acid (38.0% max.), followed by (iii) filtering to separate the ceramic particulates. The particulates were then dried and the weight fraction determined. The weight fraction was converted to

TABLE I Experimental parameters

Variable	Experiment No.				
	1	2	3	4	5
Matrix alloy	Al–Cu	Al–Cu	Al–Cu	Al–Cu	Al–Cu
Reinforcement	–	–	SiC	SiC	Al_2O_3
Atomization pressure (MPa)	1.21	1.21	1.21	1.21	1.21
Atomization gas	Ar	N_2	N_2	N_2	N_2
Superheat temperature (K)	1023	1073	1073	1073	1073
SiC carrier gas	–	–	N_2	N_2	N_2
Pressure of carrier gas (MPa)	–	–	0.17	0.17	0.17
Metal flow rate (Kg s^{-1})	0.034	0.039	0.039	0.039	0.039
Gas flow rate (Kg s^{-1})	0.013	0.018	0.018	0.018	0.018

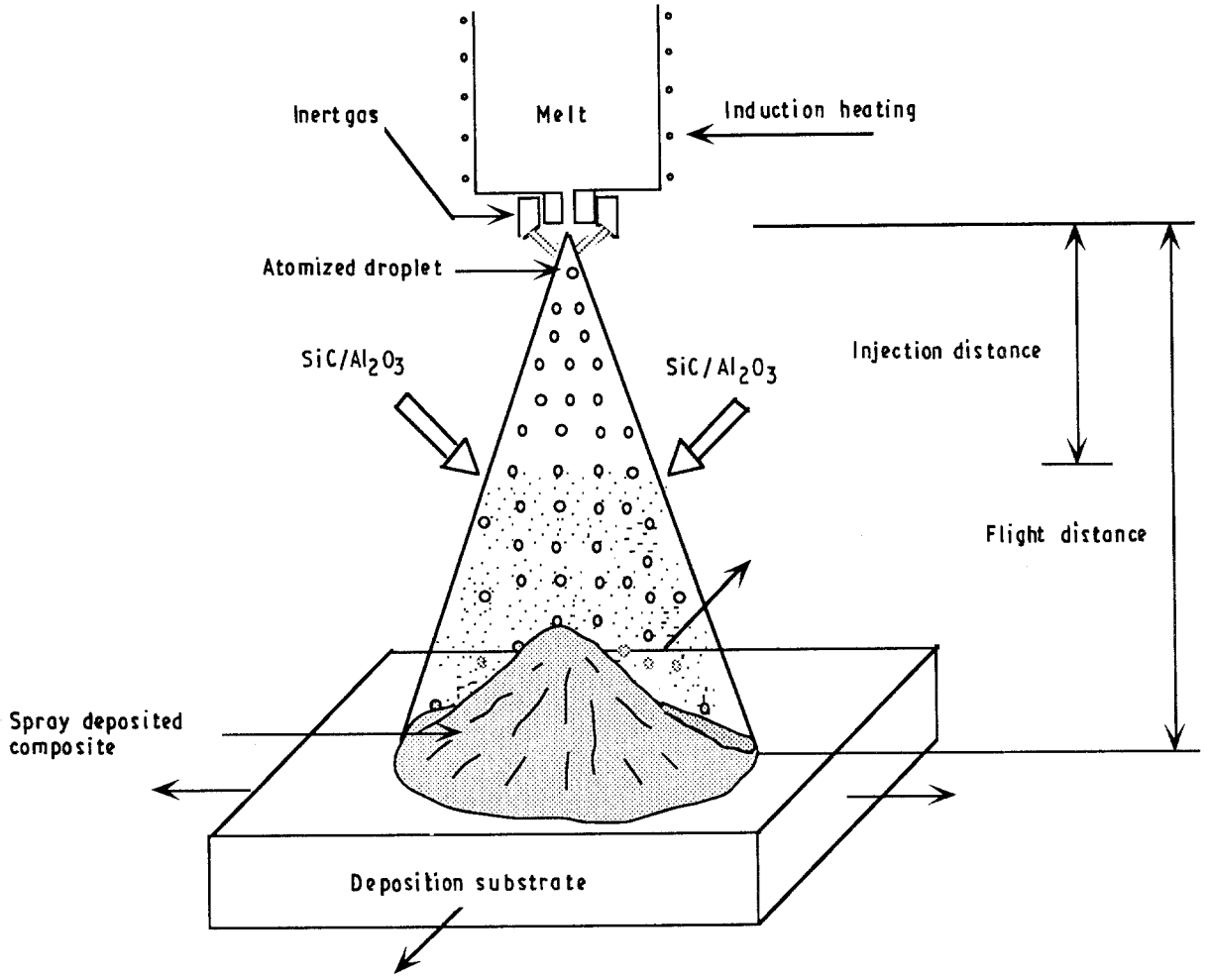

Figure 1 Schematic diagram of experimental arrangement for spray-deposition processing of metal-matrix composites.

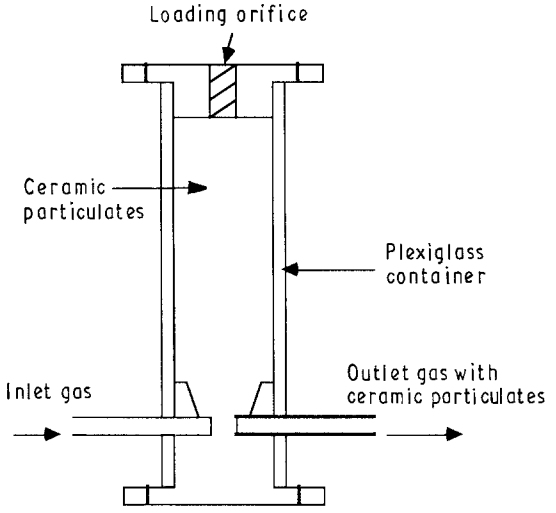

Figure 2 Schematic diagram showing coaxial tube injector.

volume fraction, $V_{f(R)}$, using the equation

$$V_{f(R)} = \frac{(\text{wt \% R})/\rho_R}{[(\text{wt \% R})/\rho_R] + [(\text{wt \% matrix})/\rho_{matrix}]} \quad (1)$$

where ρ_R and ρ_{matrix} represent the densities of the reinforcing particulates and the matrix, respectively.

Scanning electron microscopy (SEM) studies were conducted using a Hitachi S-500 microscope. Samples taken from the: (i) as-received material, (ii) as-spray deposited material, and (iii) spray-deposited and hot-extruded materials from different experiments, were sectioned to a thickness of 0.5 cm and polished using conventional techniques. The polished samples were then examined in secondary electron mode for intrinsic microstructural features. In addition, SEM studies were conducted on fractured samples taken from experiments 1, 4 and 5 in order to provide an insight into the quasi-static fracture behaviour.

Transmission electron microscopy (TEM) studies were conducted, using a Philips CM 20 microscope equipped with an energy-dispersive spectrometer (EDS) at an operating voltage of up to 120 kV, on as-spray deposited samples from experiments 2, 3 and 5. The TEM studies were carried out in order to identify SiC, Al_2O_3 and Al_2Cu (θ-type) precipitates. In addition, EDS analyses were conducted at the interfacial regions of Al–Cu/SiC and Al–Cu/Al_2O_3 in order to investigate the segregation behaviour of copper. The TEM samples were prepared using a twin-jet polisher using a 1:3 solution of HNO_3:CH_3OH at 12 V and 1.5 mA. The solution was maintained at a temperature of 263 K.

X-ray diffraction (XRD) analysis was conducted on the spray-deposited samples from experiments 2, 3 and 5 using a Philips Norelco vertical diffractometer. Thin samples were exposed to CuK_α radiation ($\lambda = 0.15418$ nm) using a scanning speed of 0.24 deg min^{-1}. A plot of intensity versus 2θ was obtained,

illustrating peaks at different Bragg angles. The Bragg angle corresponding to each of the different peaks was noted and the value of interplanar spacing, d, was calculated using Bragg's law ($\lambda = 2d\sin\theta$). The values of d obtained were matched with standard values for aluminium and other phases.

2.3. Thermomechanical treatment

Following spray processing, samples from experiments 2, 3 and 5 were isochronally annealed at 673 and 773 K in order to study the influence of temperature and annealing time on grain growth. In order to assess the mechanical behaviour, both the unreinforced and reinforced spray-atomized materials were hot-extruded. The extrusion step was accomplished using a press (capacity 82.7 MPa) at a temperature of 673 K for the unreinforced matrix material and at 723 K for the reinforced material. An area reduction ratio of 16:1 was used for all samples. The extrusion step was used in this study in order to close the micrometre-size porosity that is normally associated with spray-atomized and deposited materials [6, 7, 13]. In order to provide an insight into the ageing behaviour, Rockwell hardness measurements were made on the as-spray deposited and hot-extruded samples from experiments 1, 4 and 5, solutionized at 802 K for 2 h and isochronally annealed at 436 K for different intervals of time.

Smooth bar tensile properties were determined in accordance with ASTM E8-81. Tensile specimens were prepared from materials taken from experiments 1, 4 and 5. Tensile tests were conducted using a servohydraulic structural testing machine. The specimens were deformed at a constant crosshead speed of 0.0254 cm min^{-1}.

3. Results

3.1. Macrostructure

The overall dimensions of the spray-processed preforms from the five experiments were approximately 36 cm in length and 18 cm in width. The thickness of the preforms decreased from 5.0–7.5 cm in the central portion to approximately 0.5 cm in the thickness dimension. All of the structural characterization studies were performed on material removed from the central portion (80–90%) of the preforms. The remaining portion (10–20%) of the preforms was considered too porous for detailed analysis.

3.2. Microstructure

Optical microscopy conducted on coupons of the unreinforced matrix material taken from experiments 1 to 5 revealed the presence of an equiaxed grain morphology. The results of grain size measurements are summarized in Table II. An example taken from experiment 2 is shown in Fig. 3.

The results of density measurements revealed: (a) a density value of 2.82 g cm^{-3} for the as-received AA 2519 alloy and the extruded samples taken from experiment 1, and (b) density values for the as-extruded materials taken from experiments 4 and 5 to be 2.85 and 3.00 g cm^{-3}, respectively.

The results of the acid dissolution experiments are summarized in Table II. The volume percentages of SiC particulates present in the as-spray deposited material were estimated to be approximately 8.4 for experiment 3 and 11.1 for experiment 4, respectively. The volume percentage of Al_2O_3 for experiment 5 was approximately 16.8 for the as-spray deposited sample. The interparticulate spacings were calculated using the formula suggested by Nardone and Prewo, [20] for discontinuous reinforcement:

$$\lambda = (lt/V_f)^{1/2} \quad (2)$$

where λ is the interparticulate spacing and t, l and V_f are the thickness, length, and volume fraction of the ceramic particulates, respectively. The results of the computed interparticulate spacings, λ, are also shown in Table II.

Scanning electron microscopy of samples taken from experiment 1 revealed the presence of a finite amount of unconnected porosity and the presence of needle-shaped particles (Fig. 4). The presence of a dark region surrounding the needle-like particles is evident in the micrographs. A scanning electron micrograph taken from the as-received plates shows the plate-like morphology of these particles with a low aspect ratio (Fig. 5). The distribution of reinforcing particulates in the Al–Cu matrix is shown in Figs 6 and 7.

Transmission electron microscopy of samples taken from experiment 2 revealed a predominantly featureless matrix. The presence of nanometric-size copper-rich precipitates was noted at and along the grain

TABLE II Microstructural characterization of as-spray deposited MMCs

Experiment No.	Reinforcement size, $d50$, (μm)	Grain size (μm)	V_f (%)		Interparticulate
			Reinforcement	Porosity	spacing, (λ μm)[b]
IM[a]	–	44.0 ± 3.0	–	0.0	–
1	–	25.0 ± 2.1	–	ND[c]	–
2	–	35.5 ± 3.0	–	1.1	–
3	3	28.3 ± 2.2	8.4	ND	10.4
4	3	23.0 ± 0.5	11.1	6.9	9.0
5	3	27.7 ± 2.5	16.8	6.4	7.3

[a] Material obtained in the form of rolled plates.
[b] Values computed using Equation 2.
[c] ND: Not determined.

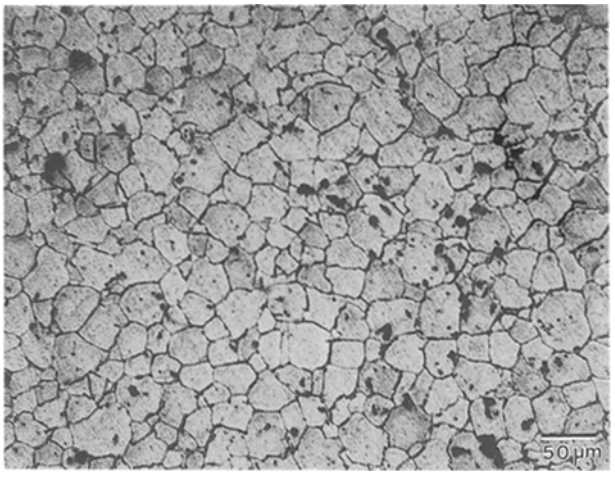

Figure 3 Optical micrograph showing equiaxed grain morphology of as-spray deposited Al–Cu sample taken from experiment 2.

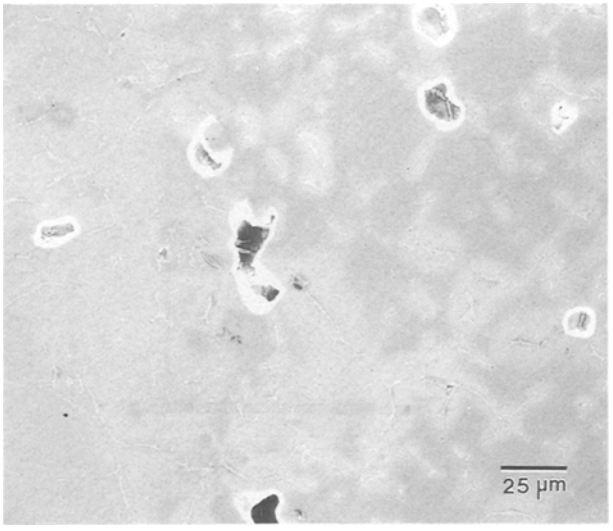

Figure 4 SEM micrograph showing the presence of unconnected porosity and needle-shaped precipitates in as-spray deposited material from experiment 1.

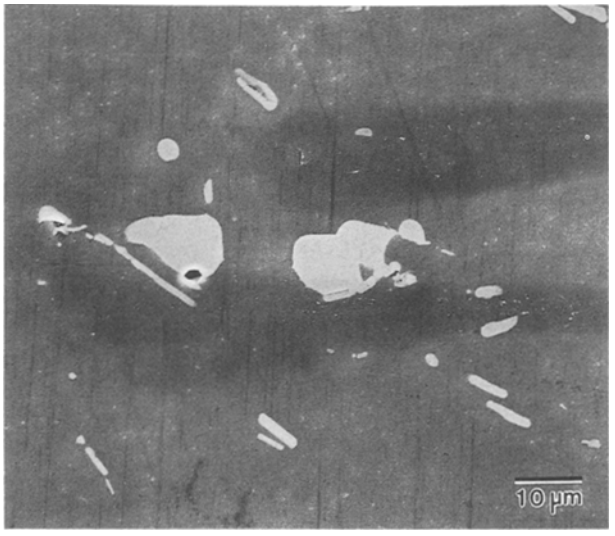

Figure 5 SEM micrograph showing the presence of plate-shaped precipitates in as-received Al–Cu rolled plates.

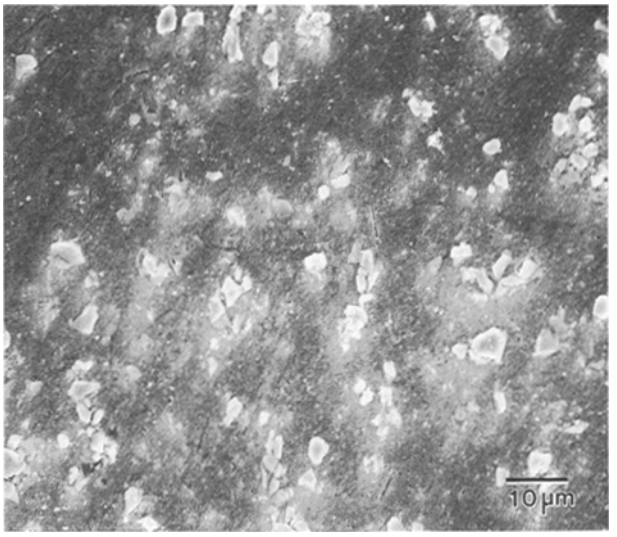

Figure 6 SEM micrograph showing the distribution of SiC particulates in as-spray deposited and extruded sample taken from experiment 4.

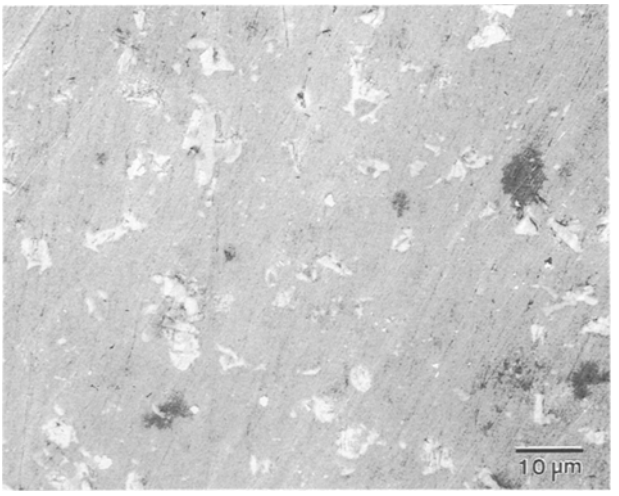

Figure 7 SEM micrograph showing the distribution of Al_2O_3 particulates in as-spray deposited and extruded sample taken from experiment 5.

boundaries (Fig. 8) and dislocation rich-areas in the matrix (Fig. 9). EDS analyses conducted on the heavily dislocated matrix regions revealed a high concentration of copper (up to 14.4 wt %). In addition, the presence of subcells was also noted in certain regions of the matrix. It is interesting to note that these regions contained approximately 8 wt % Cu, an amount that is significantly higher than that detected in dislocation-free regions. The results of TEM studies conducted on samples taken from experiment 3 revealed the presence of copper-rich precipitates at the Al–Cu/SiC interfacial region (Fig. 10). It was also observed that the interfacial precipitates were generally larger in comparison with other secondary phases that were present in the matrix. In addition, no reaction products were observed at the interface. The results of EDS analyses revealed the copper content to decrease with increasing distance from the interface (Fig. 11). The results of the TEM studies conducted on samples taken from experiment 5 revealed the presence of

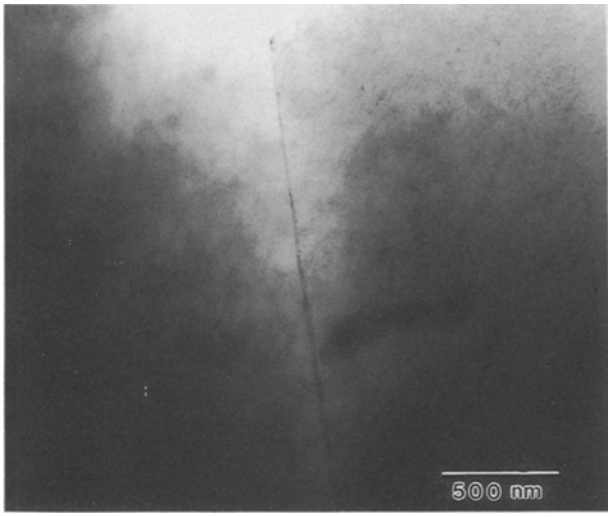

Figure 8 TEM micrograph showing the presence of nanometric-size Al_2Cu precipitates at the grain boundary observed in samples taken from experiment 2.

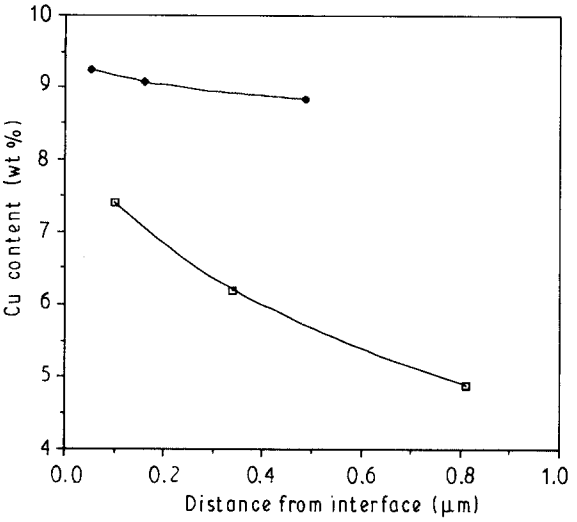

Figure 11 Graphical representation of the segregation pattern at (⊡) Al–Cu/SiC and (◆) Al–Cu/Al_2O_3 interfacial regions observed in samples taken from experiments 3 and 5.

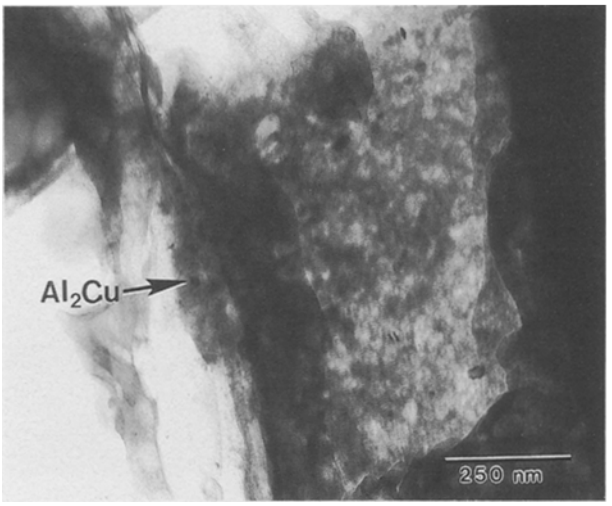

Figure 9 TEM micrograph showing the presence of nanometric-size Al_2Cu precipitates in the dislocation-rich area of the matrix observed in samples taken from experiment 2.

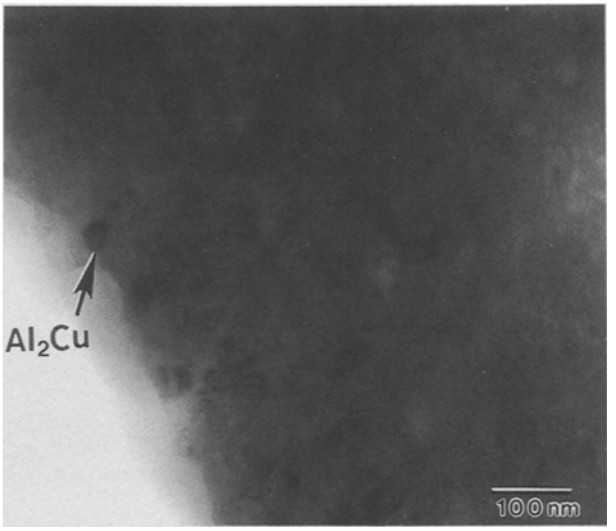

Figure 12 TEM micrograph showing the presence of nanometric-size Al_2Cu precipitates observed in samples taken from experiment 5.

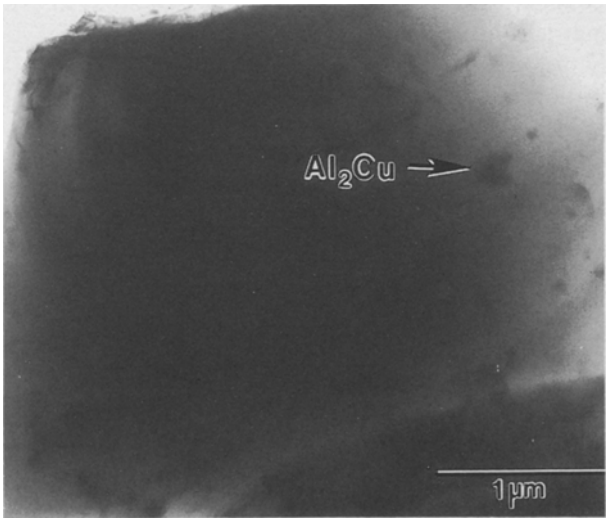

Figure 10 TEM micrograph showing the presence of nanometric-size Al_2Cu precipitates at the Al–Cu/SiC interfacial region observed in samples taken from experiment 3.

copper-rich precipitates in the matrix. The size and morphology of these precipitates were similar to those that were observed in samples taken from experiments 2 and 3 (Figs 9, 10 and 12). Efforts to establish the precise identity of copper-containing precipitates observed in samples taken from experiments 2, 3 and 5 were not successful. However, on the basis of the equilibrium phase diagram [21] and the X-ray diffraction results, these precipitates are likely to be of the Al_2Cu type (θ-type). The results obtained from EDS analyses conducted at various distances from the Al–Cu/Al_2O_3 interface are summarized in Fig. 11. The results reveal the Al–Cu/Al_2O_3 interfacial region to be more enriched in Cu, when compared to the interfacial region of the Al–Cu/SiC metal matrix composite (see Fig. 11).

The X-ray diffraction spectra corresponding to as-spray deposited samples from experiments 2, 3 and 5 were analysed. The lattice spacings (d) corresponding to the observed Bragg angles are shown in Table III.

TABLE III Results of X-ray diffractometry studies

Experiment 2 (Al–Cu)								
2θ (deg)	38.38	42.58	44.67	47.09	47.74	65.16	78.38	
Calculated *d* value (nm)	0.234	0.212	0.203	0.193	0.190	0.143	0.122	
Experiment 3 (Al–Cu/SiC)								
2θ (deg)	34.16	35.68	38.56	42.60	42.68	44.76	47.36	60.08
Calculated *d* value (nm)	0.262	0.251	0.233	0.212	0.211	0.202	0.191	0.154
Experiment 5 (Al–Cu/Al_2O_3)								
2θ (deg)	35.16	38.56	43.40	44.80	57.48			
Calculated *d* value (nm)	0.255	0.233	0.208	0.202	0.160			
Standard *d* values (nm)								
Al	0.2338	0.2025	0.1432	0.1221	0.1169			
α-Al_2O_3	0.255	0.209	0.160					
Al_2Cu	0.191	0.212	0.429					
α-SiC	0.251	0.263	0.154					

The XRD spectrum corresponding to the as-spray deposited Al–Cu material (experiment 2) indicated the presence of pure aluminium and Al_2Cu phases. The XRD spectrum corresponding to the as-spray deposited Al–Cu/SiC material (experiment 3) indicates the presence of pure aluminium, Al_2Cu and α-SiC phases, while the XRD spectrum corresponding to the Al–Cu/Al_2O_3 composite material (experiment 5) revealed the presence of pure aluminium and α-Al_2O_3 phases.

3.3. Grain growth behaviour

In order to provide an insight into the effects of the SiC and Al_2O_3 particulates on the microstructure of the composite matrix during solid-state cooling, grain growth studies were conducted on the samples taken from experiments 2, 3 and 5. The grain sizes were determined using the linear intercept method, after isochronal anneals at 673 and 773 K (Tables IV and V and Figs 13 and 14). The results of grain size measurements shown in Figs 13 and 14 reveal a logarithmic progression of grain growth with time for the unreinforced Al–Cu, and reinforced Al–Cu/SiC and Al–Cu/Al_2O_3 materials. Not unexpectedly, it can be seen that the final grain sizes of the Al–Cu/SiC and Al–Cu/Al_2O_3 composite materials, at 673 and 773 K, are lower than that of the unreinforced matrix material. The microstructure of the as-spray deposited monolithic alloy (Al–Cu) and the SiC- and Al_2O_3-reinforced Al–Cu matrices consisted of equiaxed grains, both before and after the isochronal heat treatments.

3.4. Ageing studies

The results of the ageing studies conducted on samples removed from experiments 1, 4 and 5 are shown in Fig. 15. The results exhibit the presence of a well-defined peak at 12.0 h for the samples taken from experiments 1, 4 and 5. The results also reveal that the maximum peak hardness is achieved in samples taken from experiment 4 followed by samples taken from experiments 5 and 1, respectively. In addition, the results also show the as-quenched hardness of the composites samples to be higher than the monolithic counterpart.

TABLE IV Results of grain size measurements for different intervals of time at 673 K for as-spray atomized and deposited samples of Al–Cu, Al–Cu/SiC and Al–Cu/Al_2O_3 materials

Time (min)	Grain size (μm)		
	Experiment 2	Experiment 3	Experiment 5
0[a]	35.5 ± 3.0	28.3 ± 2.2	27.7 ± 2.5
1	36.6 ± 3.8	28.7 ± 1.1	28.3 ± 0.9
10	39.5 ± 1.8	31.5 ± 1.0	31.1 ± 0.7
50	43.0 ± 1.3	34.2 ± 0.91	35.0 ± 0.8
100	44.8 ± 2.1	38.8 ± 0.6	35.1 ± 2.2

[a] Time 0 refers to as-spray deposited grain size.

TABLE V Results of grain size measurements for different intervals of time at 773 K for as-spray atomized and deposited samples of Al–Cu, Al–Cu/SiC and Al–Cu/Al_2O_3 materials

Time (min)	Grain size (μm)		
	Experiment 2	Experiment 3	Experiment 5
0[a]	35.5 ± 3.0	28.3 ± 2.2	27.7 ± 2.5
1	37.8 ± 8.0	29.1 ± 1.8	29.3 ± 1.6
10	39.9 ± 2.6	35.2 ± 4.7	34.7 ± 2.3
50	46.2 ± 2.3	36.2 ± 1.4	37.5 ± 1.0
100	48.8 ± 2.7	39.1 ± 1.2	42.2 ± 2.8

[a] Time 0 refers to as-spray deposited grain size.

3.5. Mechanical behaviour

The results of ambient-temperature testing on the spray-deposited and hot-extruded unreinforced and reinforced matrices (Al–Cu), aged to peak hardness, are summarized in Table VI. Also shown in this table are the properties of equivalent material prepared by the ingot metallurgy route. The results in Table VI reveal that the ambient-temperature mechanical properties of the unreinforced spray-deposited materials accord well with those of the ingot metallurgical material [22]. The results also show that the presence of particulate reinforcement (SiC or Al_2O_3) in the

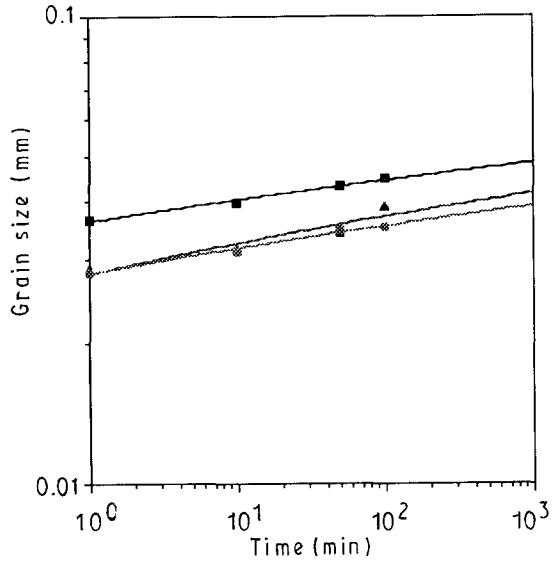

Figure 13 Graphical representation of the logarithmic grain growth relationship at 673 K observed in as-spray deposited (■) Al–Cu, (▲) Al–Cu/SiC and (●) Al–Cu/Al_2O_3 materials.

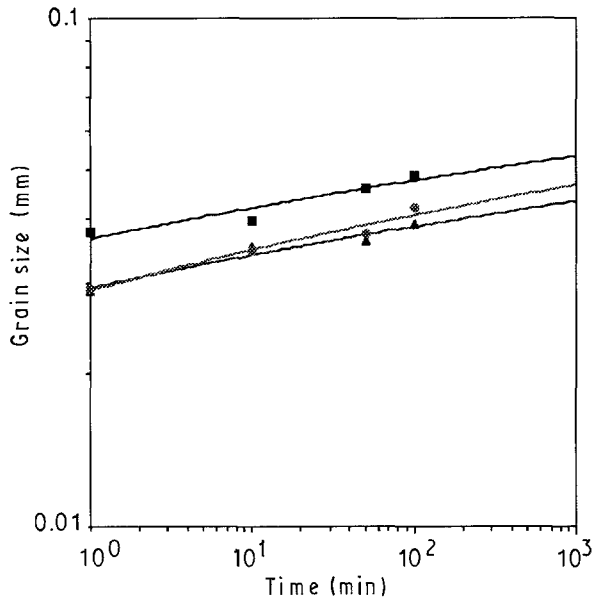

Figure 14 Graphical representation of logarithmic grain growth relationship at 773 K observed in as-spray deposited (■) Al–Cu, (▲) Al–Cu/SiC and (●) Al–Cu/Al_2O_3 materials.

Al–Cu matrix does not help in improving strength, and, in fact, degrades the ductility of the composite matrices.

3.6. Fracture behaviour

Macroscopic investigation of the fracture surfaces of samples taken from experiment 1 reveal the presence of a cup and cone type of fracture. Fig. 16 is a representative scanning electron micrograph showing the morphology of the fracture surface. The presence of dimples of uniform size is indicative of ductile failure. Fracture surfaces samples of the SiC-reinforced composites (experiment 4) reveal matching fracture surfaces tilted at an angle of $\sim 8^\circ$ with respect to the horizontal plane, suggestive of brittle failure. Fig. 17a is a low-magnification scanning electron micro-

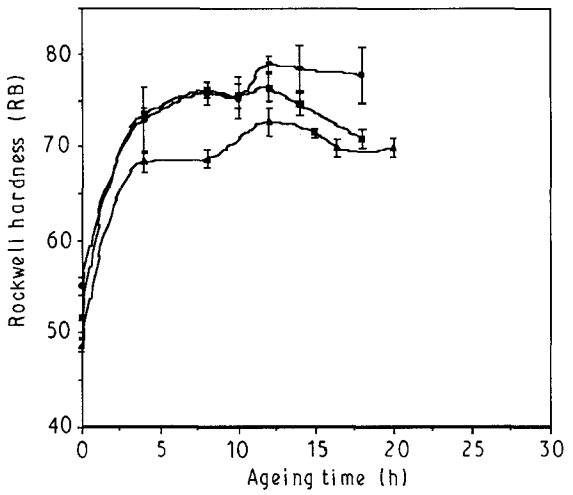

Figure 15 Graphical representation of ageing studies conducted on as-spray deposited and extruded (▲) Al–Cu (experiment 1), (●) Al–Cu/SiC (experiment 4) and (■) Al–Cu/Al_2O_3 (experiment 5). All materials were solution-treated at 802 K for 2 h.

TABLE VI Results of room-temperature mechanical properties

Experiment No.	YS (MPa)	UTS (MPa)	Ductility (%)
1	318.7 ± 0.0	410.3 ± 10.7	14.7 ± 0.7
4	301.2 ± 5.3	422.3 ± 8.5	10.8 ± 0.5
5	299.6 ± 4.6	411.8 ± 5.3	6.5 ± 1.3
IM	332.3[a]	–[b]	–[b]

[a] Cast samples solutionized at 802 K and aged at 436 K for 16 h [22].
[b] Not reported.

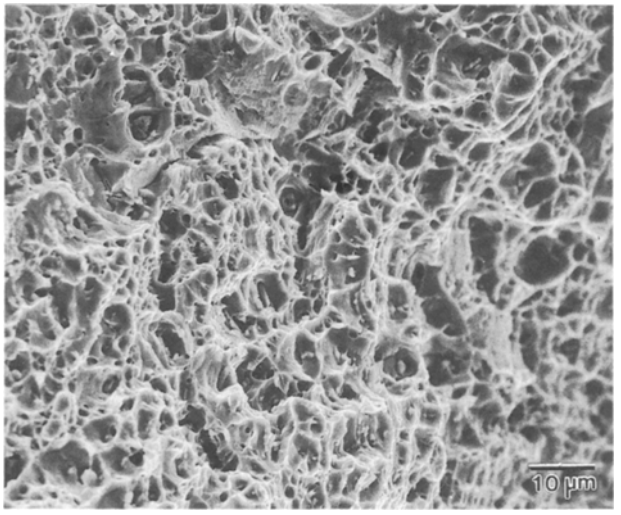

Figure 16 SEM micrograph showing fracture surface morphology of sample taken from experiment 1.

graph of the fractured sample. Cracks can be seen emanating and randomly distributed throughout the fracture surface. Fig. 17b shows regions of highly localized plastic deformation and that of brittle failure on the fracture surface of a sample taken from experiment 4. In addition, interfacial debonding was observed between SiC particulates and the matrix, in the sample taken from experiment 4 (Fig. 18). Finally,

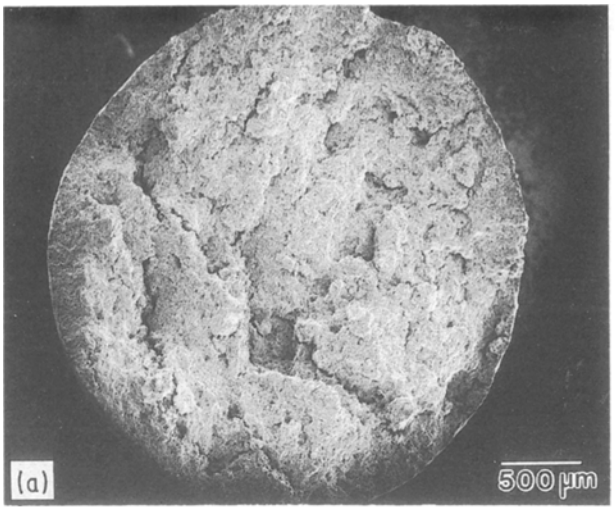

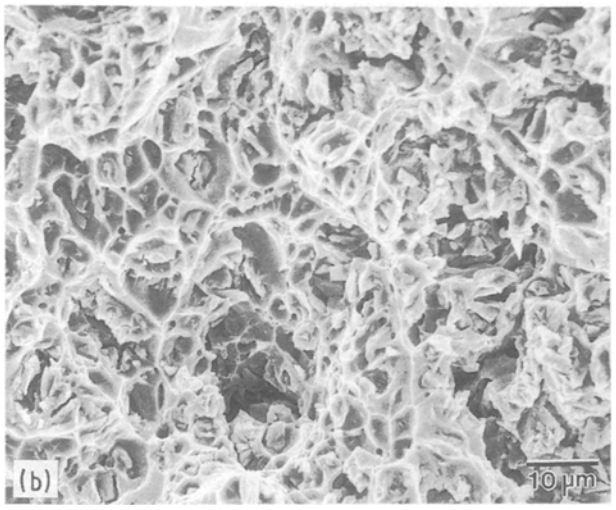

Figure 17 Representative SEM micrographs showing (a) cracks distribution on the fracture surface and (b) mixed-mode type of failure observed in fractured samples taken from experiment 4.

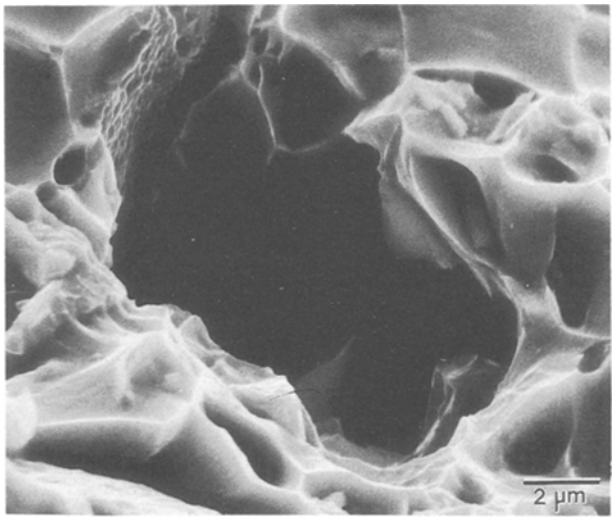

Figure 18 SEM micrograph showing the interfacial debonding between matrix and SiC reinforcement observed on the fractured surface of sample taken from experiment 4.

macroscopic examination of the fractured samples taken from experiment 5 revealed the fractured surfaces to be tilted by $\sim 7°$ to the horizontal plane, suggestive of brittle failure. Fig. 19a is a low-magnification scanning electron micrograph revealing the presence of cracks randomly distributed throughout the fracture surface. Fig. 19b is a representative scanning electron micrograph revealing a mixed-mode type of fracture. The regions corresponding to highly localized plastic deformation and features reminiscent of brittle failure can easily be discerned in this figure.

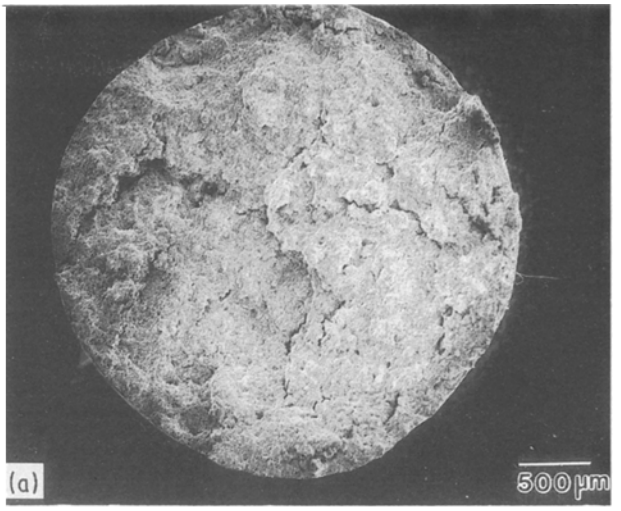

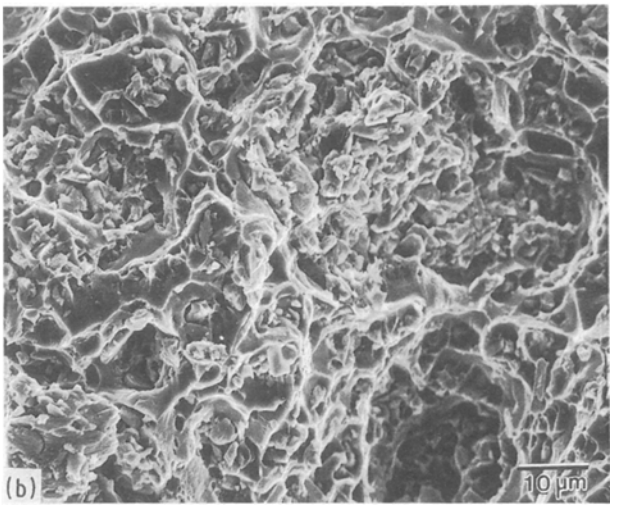

Figure 19 Representative SEM micrographs showing (a) crack distribution on the fracture surface and (b) mixed-mode type of failure observed in fractured samples taken from experiment 5.

Finally, the presence of cavities of ~ 5 to ~ 15 μm were observed on the fractured surfaces of the samples taken from experiments 4 and 5. These cavities were noted to be associated with either the large ceramic particulates or clusters of small particulates.

4. Discussion

4.1. Microstructure

Three salient features are associated with the microstructure of spray-atomized and co-deposited ceramic particulate-reinforced metal-matrix composites:

(a) the grain structure,
(b) the presence of micrometre-sized pores, and
(c) the amount and distribution of reinforcing particulates.

The grain morphology of the spray-atomized and co-deposited MMCs was equiaxed, in agreement with the results obtained by other investigators [23–31]. The mechanisms associated with the formation of equiaxed grains during spray atomization and deposition processing are addressed elsewhere [6, 23–27, 31], and will not be reiterated here. The results from Table II reveal the experimentally observed grain sizes for the unreinforced and reinforced spray-deposited materials to range from 23.0 to 35.5 μm. The relatively finer-grained microstructure noted for experiment 1 (25.0 μm), relative to that obtained in experiment 2 (35.5 μm), is consistent with the lower superheat temperature used in experiment 1 (1023 K), relative to that used in experiment 2 (1073 K) [32]. The results also show that increasing the volume fraction of reinforcement effectively decreases the grain size of the as-spray deposited material as observed in experiments 2, 3 and 4 (see Table II). Moreover, the results convincingly show that the grain size of the as-received plates is higher than that observed for the unreinforced and reinforced materials, in the as-spray deposited condition. Finally, it can be seen that the presence of 11.1% (V_f) of SiC particulates in the metal matrix is far more effective in refining the grain size when compared to 16.8% (V_f) of Al_2O_3, under identical processing conditions (Table II). A thorough discussion of the effects of the processing variables on the resulting microstructure obtained during spray atomization and deposition is provided elsewhere [6, 7, 27].

A second important microstructural characteristic frequently associated with spray-atomized and deposited microstructures is the presence of a finite amount of non-interconnected porosity [23–30]. The overall amount of porosity present in spray-atomized and deposited materials depends on the following:

(a) the thermodynamic properties of the material,
(b) the thermodynamic properties of the gas, and
(c) the processing parameters.

Under conditions typical for aluminium alloys, the amount of porosity present in spray-atomized and deposited materials has been reported to be in the 1–10% range [6, 23, 25] (Fig. 4). The various mechanisms governing the formation of pores during spray atomization and deposition can be found elsewhere [33–36]. Finally, the results of this study reveal that the presence of ceramic particulates (SiC/Al_2O_3) increases the volume fraction of porosity in the as-spray deposited materials when compared to that of the unreinforced matrix material, processed under identical conditions (Table II). This is attributed in part to enhanced heat transfer and the concurrent increase in solid fraction of the droplets prior to deposition [13].

The resultant size, amount and distribution of reinforcing particulates is of interest since the mechanical behaviour of the ceramic particulate-reinforced metal-matrix composites is linked with the presence of these particulates in the matrix. The volume fraction of ceramic particulates present in spray-atomized and co-deposited materials has been correlated with processing parameters such as injection angle, injection pressure and ceramic/metal mass flow ratio, and physical properties such as surface tension of the atomized droplets [23, 25, 37, 38]. The ceramic particulates may be incorporated into the aluminium alloy matrix by two possible mechanisms:

(a) the ceramic particulates penetrate the atomized droplets during co-injection and remain entrapped in the matrix during subsequent impact with the deposition surface [38], or
(b) the SiC particulates remain on the surface of the atomized droplets and are entrapped by the matrix after impact with the deposition surface.

Gupta *et al.* [6, 27] proposed that the extent of particulate entrapment after impact will depend on the conjunct influence of the magnitude of impact and repulsive forces present at the metal–ceramic interface. If entrapment fails to take place either during co-injection, or subsequently, during deposition, the microstructure of the spray-atomized and co-deposited materials will be characterized by a high concentration of ceramic particulates at the prior droplet boundaries. Such a situation has been reported by Ibrahim *et al.* [39] for a spray-atomized and deposited 6061 Al/SiC metal-matrix composite.

A comparison of the observed grain sizes with the measured interparticulate spacings provides an insight into the extent of entrapment that occurred during the experiments (Table II). The results show that the interparticulate spacings in materials from experiments 3, 4 and 5 were substantially smaller than the measured grain sizes, suggesting entrapment of the ceramic particulates by a large proportion of the droplet population. However, on the basis of the present data, it was not possible to discern whether the entrapment of the ceramic particulates occurred during atomization, or during subsequent deposition. Furthermore, it is worth noting that the SiC particulates were more homogeneously distributed in the Al–Cu metal matrix when compared to the Al_2O_3 particulates. The Al_2O_3 particulates showed a tendency to agglomerate into clusters (Fig. 7). Further work continues in this area.

On the basis of the present experimental findings, it appears that the co-injection of ceramic particulates during deposition influences the precipitation kinetics. Phase equilibria, as inferred from the Al–Cu phase diagram [21], is consistent with the XRD results obtained for experiments 2 and 3, which confirmed the presence of Al_2Cu precipitates. However, failure to detect the presence of Al_2Cu-type phases using SEM in samples taken from experiment 3 suggests that the precipitates were refined by the presence of reinforcing phases. This phenomenon is consistent with the results of Salvo *et al.* [40] who suggested that the finer precipitate size that is commonly observed in MMCs may be attributed to a greater number of nucleation sites associated with a higher density of dislocations that is present in the reinforced metal matrices. Finally, failure to detect Al_2Cu diffraction lines in samples taken from experiment 5 is ascribed to two competing reasons:

(a) the volume fraction of Al_2Cu is below the XRD detection limit, and/or

(b) precipitation of Al_2Cu is completely suppressed.

The latter phenomenon is unlikely as a result of the high quench rates that are necessary to completely suppress this reaction. In related studies, it has been suggested that the formation of microsegregation-free solidification is governed by either the absolute stability criterion or solute trapping [41–43]. In order to achieve considerable solid solubility extension, the amount of solute C has to be less than a critical amount C_{cr}. If $C < C_{cr}$, the formation of microsegregation-free solidification will be governed by the absolute stability criterion and substantial extension of solid solubility can be realized. However, if $C > C_{cr}$, the formation of microsegregation-free solidification will be governed by solute trapping and the material system will exhibit a relatively high resistance to solid solubility extension. In order to analyse the present system, C_{cr} was computed by considering the alloy as a simple binary Al–Cu system, on the basis of the following equation [41–43]:

$$C_{cr} = \frac{k^2\Gamma}{m_L(1-k)a_o} \quad (3)$$

where m_L is the liquidus slope, k is the partition coefficient, Γ is the Gibbs–Thompson coefficient and a_o is the interatomic distance. The values of k (0.16) and m_L (3.4 K/wt %) were taken from Murray [44], while the value of $\Gamma = 1.08 \times 10^{-7}$ K m was taken from Juarez Islas *et al.* [45]. Substitution of these values in Equation 3 predicts the value of C_{cr} to be 2.39 wt % Cu. Hence, for the alloy used $C > C_{cr}$ and the formation of microsegregation-free solidification will be governed by solute trapping. Moreover, in view of results provided and discussed elsewhere [6, 46], which suggest that the solidification front velocity during spray atomization and deposition is of the order of 1–2 mm s^{-1}, it is unlikely that complete suppression of copper precipitation as Al_2Cu occurred in this study. The results of our analyses are consistent with TEM observation of samples taken from experiment 5. The results show the presence of Al_2Cu-type precipitates in the matrix (Fig. 12). Quantitative analyses to determine the size distribution and volume fraction of these precipitates could not be conducted due to difficulties associated with

(a) non-uniform distribution of precipitates,

(b) nanometric size of the precipitates, and

(c) sample area investigated.

The reduction in intensity (as observed in experiment 3) and the absence of diffracted beams (as observed in experiment 5) corresponding to Al_2Cu may be attributable to a decrease in growth kinetics experienced by the Al_2Cu precipitates, as a result of an enhancement in heat transfer brought about by the presence of ceramic particulates, during deposition [26].

4.2. Solid-state cooling effects

Once the mixture of solid, liquid and mushy droplets impacts the deposition substrate, the newly formed grains will continue to grow during solid-state cooling. In order to gain an insight into the growth of grains in both the reinforced matrix and unreinforced matrix, kinetic analysis of the data, given in Tables IV and V, was used to calculate the grain growth exponent in the as-spray deposited materials. The grain growth exponent n represents the slope of the line when the grain size (mm) is plotted as a function of time (min) on a bilogarithmic plot [47–49]. The empirical relationship correlating grain size with annealing time and grain growth exponent can be expressed as

$$D = C(t)^n \quad (4)$$

where D is the average grain diameter, t is the annealing time, and C and n are constants. The numerical values of C and n depend on both alloy composition and annealing temperature (Table VII). The values of n have been reported to range from 0.05 to 0.50 [50]. A comprehensive discussion of the significance of the exponent n can be found elsewhere [50, 51]. The main assumptions involved in the development of Equation 4 are:

(a) the grains have an equiaxed morphology,

(b) there is no prior deformation, and

(c) the grain growth is normal [47–49].

Regarding the grain morphology, the presence of equiaxed grains has been established in the preceding section. Finally, the linear relationship observed between grain growth and annealing time (Figs 13 and 14) provides an experimental basis for the assumption of normal growth.

A few comments are in order regarding the values of grain growth exponent n obtained in this study. It is observed (Table VII) that the value of n for a constant temperature is lower for the Al–Cu material (0.044–0.056) relative to those of the Al–Cu/SiC (0.059–0.060) and Al–Cu/Al_2O_3 (0.050–0.074) composite materials. Furthermore, the results also reveal the value of n to increase with an increase in temperature for the unreinforced and reinforced materials, consistent with the results obtained by other investigators [50, 51]. This behaviour is rationalized by considering the extrinsic and intrinsic effects associated with the co-injection of ceramic particulates.

The co-injection of the ceramic particulates during spray atomization and deposition increases the rate of heat transfer from the atomized spray and, thereby, promotes the retention of alloying elements in solid solution in the matrix [26]. In related studies, Gupta

TABLE VII Results of grain growth exponents

Experiment No.	Temperature (K)	C	n
2	673	0.036	0.044
	773	0.037	0.056
3	673	0.028	0.059
	773	0.029	0.060
5	673	0.028	0.050
	773	0.029	0.074

et al. [52] used X-ray diffractometry to show that a spray-processed Al–4.0 Ti material retained 0.88 wt % Ti in solid solution, whereas the corresponding as-spray processed Al–2.3 wt % Ti/SiC material retained up to 1.13 wt % Ti in solution. An excess solid solubility of the alloying elements in the matrix will tend to reduce the volume fraction of precipitates in the matrix and, in effect, allow for easier grain boundary mobility. This rationale is supported by the results of X-ray diffraction studies which failed to reveal the presence of Al_2Cu-type precipitates in the as-spray processed Al–Cu/Al_2O_3 composite samples. Hence, on the basis of the results obtained, it appears that the presence of Al_2Cu-type precipitates in the matrix inhibits grain growth more effectively than the reinforcing ceramic particulates.

4.3. Ageing studies

The results of this study reveal that the as-quenched hardness of the metal-matrix composites is higher than that of the monolithic counterpart. This is attributed in part to the high dislocation density present in the composite matrix due to the mismatch between the coefficients of thermal expansion of the metal matrix and the ceramic reinforcement [53]. The results also show that the ageing time for peak hardness was the same for the unreinforced Al–Cu and reinforced Al–Cu/SiC and Al–Cu/Al_2O_3 materials. These results are consistent with the findings and observations of Chawla *et al.* [54] and Salvo *et al.* [40]. These researchers showed a negligible difference in ageing kinetics between unreinforced and reinforced materials when they were aged at relatively low temperatures ($\sim$423 K). Moreover, in related studies conducted on aluminium alloy 6061, Rack and Krenzer [55] showed that in some instances the ageing kinetics of unreinforced material may even be faster than for the reinforced materials due to changes in the precipitation sequence, caused by the presence of a large number of matrix dislocations. This behaviour has also been reported for spray-processed 6061 composites during a time interval of $0.6 > t > 0.0$ h [56]. In addition, the higher hardness observed for the SiC-reinforced composites, as compared to the Al_2O_3-reinforced composites in both the as-quenched and peak-aged conditions, can be attributed to the higher hardness of SiC (Vickers hardness 3000–3500 kg mm^{-2}) as compared to Al_2O_3 (Vickers hardness 2600 kg mm^{-2}) [57]. These results are consistent with the work of Salvo *et al.* [40] who studied 6061 aluminium alloy reinforced with SiC and Al_2O_3 particulates, and processed using a compocasting technique.

4.4. Mechanical behaviour

The results of the mechanical behaviour studies indicate that the co-injection of SiC or Al_2O_3 particulates in the Al–Cu matrix reduces the yield strength (YS) and ductility of the matrix material and does not significantly improves the ultimate tensile strength (UTS). The reduction in UTS values for the metal-matrix composites is not unusual and has also been reported by several other investigators [28, 39, 58]. In related studies, Ibrahim *et al.* [39] showed that strength of a metal-matrix composite increased appreciably over that of the monolithic counterpart only when the volume fraction of the reinforcing particulates was increased over 28%. Friend [59] suggested that unless there is a critical volume fraction of reinforcing phase in the matrix, the load transfer between the matrix and the reinforcement will not be effective and a concomitant strength improvement may not be realized.

To provide an insight into the strengthening behaviour of the MMCs used in this study, a simple numerical formulation was developed. The objective of this formulation was to calculate the critical volume fraction of reinforcing particulates required above which strengthening is to be expected in discontinuously reinforced metal matrices. The model formulation incorporates the following important assumptions:

(a) the reinforcing particulates are equiaxed (e.g. aspect ratio = 1),
(b) the reinforcing particulates acts as load carriers until the onset of debonding, and
(c) the reinforcing particulates are uniformly distributed in the matrix.

The strength of MMCs may be estimated on the basis of rule-of-mixture theory for uniaxial continuous fibre composites as [59]

$$\sigma_c = \sigma_{uf} V_f + \sigma_m^*(1 - V_f) \quad (5)$$

where σ_c is the composite strength, σ_{uf} the strength of reinforcing phase and σ_m^* the matrix stress at the reinforcement failure strain.

Equation 5 needs to be modified in order to account for the presence of surface flaws that are typically associated with the reinforcing ceramic phase. For example, the presence of the sharp edges on ceramic particulates, with concomitant stress concentration effects, is known to promote early void nucleation [60]. Moreover, the occurrence of interfacial debonding has also been shown to play a critical role in the deformation behaviour of metal-matrix composites [61]. In view of these findings Equation 5 was modified to account for the fact that composite strength is intimately linked to the strength of the interface. Hence, replacing σ_{uf} by σ_i

$$\sigma_c = \sigma_i V_f + \sigma_m^*(1 - V_f) \quad (6)$$

where σ_i is the interfacial bond strength between the soft and ductile matrix and the hard and brittle reinforcement.

Now in the limit, when the volume fraction of reinforcement V_f equals the critical volume fraction V_{CRIT}, the strength of the composite σ_c will be equal to that of the unreinforced matrix material σ_{mu}. Hence we can write Equation 6 as

$$\sigma_{mu} = \sigma_i V_f + \sigma_m^*(1 - V_f) \quad (7)$$

where σ_{mu} is the ultimate strength of the unreinforced matrix. Replacing V_f by V_{CRIT} and rearranging

Equation 7 we obtain

$$V_{CRIT} = \frac{\sigma_{mu} - \sigma_m^*}{\sigma_i - \sigma_m^*} \quad (8)$$

On the basis of work discussed elsewhere [11, 62, 63], an interfacial bond strength value of $\sigma_i = 1690$ MPa was used to calculate V_{CRIT} for the SiC particulate-reinforced metal-matrix composites used in this study. A similar calculation was not attempted for the Al_2O_3 particulate-reinforced metal-matrix composites due to the unavailability of a σ_i value for this material. The results of this calculation, summarized in Table VIII, suggest that $V_{CRIT} = 8.2\%$ for the SiC particulate-reinforced MMCs. The small difference between the calculated V_{CRIT} (8.2%) and the actual V_f (11.1%) is consistent with the marginal improvement in strength that was experimentally observed. The computed value of V_{CRIT}, however, should be considered as a lower-bound estimate since, in practice, a completely uniform distribution of reinforcing particulates in the metal matrix is difficult to achieve, and hence there are always clusters or agglomeration sites present in the matrix which promote early crack nucleation. This is consistent with the presence of cavities (5–15 μm) that were noted on the fracture surfaces of some of the MMC samples. These cavities are thought to originate as a result of the interfacial debonding originating at clusters of reinforcing ceramic particulates. The calculated value of V_{CRIT}, however, provides an insight into the minimum volume fraction of reinforcement that is required to realize an improvement in strength in discontinuously reinforced MMCs. Moreover, inspection of Equation 8 reveals some interesting trends. First, Equation 8 suggests that the higher the bond strength σ_i, the lower the volume fraction of ceramic reinforcement that is required for an improvement in strength. Secondly, an increase in the matrix strength σ_{mu} is accompanied by an increase in V_{CRIT}. Regarding the first observation, a high value of σ_i is indicative of a more effective matrix–reinforcement load transfer. Hence, the MMC will need a smaller volume fraction of reinforcement relative to one with a poorly bonded reinforcement (e.g. low σ_i). The second observation is consistent with the results reported by McDanels [64] for 20 vol % SiC_w/Al. In this study, he noted the strength improvement that was realized in a 6061 MMC to be higher than that noted for 2124 and 7075 MMCs, consistent with the lower matrix strength of the 6061 alloy relative to alloys 2124 and 7075.

Regarding the effect of the type of reinforcement on the mechanical behaviour of the spray-deposited MMCs, a few comments are in order. Inspection of Fig. 11 suggests that the interfacial region of the Al_2O_3-reinforced metal-matrix composite exhibits a higher concentration of Cu when compared to that of the SiC-reinforced metal-matrix composite. The Cu enrichment at the interface will deplete the adjacent matrix of Cu, thereby leading to a lower volume fraction of Al_2Cu-type precipitates (primary strengthening phase) during subsequent ageing, and thus possibly weakening the matrix. This suggestion is consistent with the relatively small difference in tensile strength between the MMCs and the unreinforced matrix materials, noted in this study. Moreover, the higher segregation of Cu noted in the Al_2O_3-reinforced MMC, relative to that in the SiC-reinforced MMC is consistent with the higher strength improvement observed in the latter material relative to that in the former. This is despite the fact that the volume fraction of Al_2O_3 (16.8%) exceeded that of the SiC (11.1%). It should be noted, however, that the overall strength of the MMCs is not solely dictated by constitutional changes in the matrix brought about by the presence of ceramic reinforcements, but also governed by competing influences of: structural changes in the matrix [65, 66], volume fraction and distribution of ceramic reinforcement [67], defect concentration in reinforcement [66], and the extent of interfacial bonding between the matrix and reinforcement [68].

TABLE VIII Input parameters and the results of numerical model

Variable	Value
σ_i (MPa)	1690.0
σ_m^* (MPa)[a]	361.4
σ_{mu} (MPa)	470.6
V_{CRIT} (%)	8.2

[a] Assuming 0.67% strain to failure.

4.5. Fracture behaviour

The extent of brittle fracture, as determined from fractographic studies, ranged (in ascending order) from unreinforced matrix to SiC-reinforced MMC to Al_2O_3-reinforced MMC. These results are consistent with the mechanical properties (Table VI) which show a maximum ductility of 14.7% for the unreinforced matrix material and a minimum ductility of 6.5% for Al_2O_3-reinforced matrix. In addition, the relatively uniform and finer dimple size of the unreinforced material as compared to the reinforced counterparts (experiments 4 and 5) are indicative of ductile failure [64]. The extent of particulate breakage and interfacial debonding noted on the fracture surface of samples taken from experiment 4 is consistent with results obtained in earlier studies on SiC-reinforced Al–7Si [61]. The relatively low difference in atomic contrast between the Al_2O_3 particulates and the matrix made it difficult to analyse the fracture surface of samples taken from experiment 5 with respect to interfacial debonding and particulate breakage.

5. Conclusions

1. The results of grain size measurements and grain growth studies conducted on the as-spray processed materials indicate that silicon carbide (SiC) particulates are more effective in refining grain size than the aluminium oxide (Al_2O_3) particulates.

2. The ageing kinetics of the spray-processed and hot-extruded MMCs remain the same as those of the monolithic material.

3. The results of the present study also show that the presence of particulate reinforcement (SiC or Al_2O_3)

in the aluminium alloy matrix (AA 2519) does not help in improving strength, and, in fact, reduces the ductility of the composite material.

4. Regarding strengthening behaviour, preliminary results obtained, on the basis of a simple numerical formulation, suggest that a minimum of 8.2 vol % of SiC particulates is required in order to realize a strength improvement for the Al–Cu matrix material used in this study.

Acknowledgements

The authors wish to acknowledge the Army Research Office (grant DAALO3-92-G-0181) for their financial support. In addition, the authors would like to thank Mr Irwin Sauer for his assistance with the experimental part of the study, and Dr Grace K. Goo for her help in conducting TEM studies.

References

1. P. S. GILMAN, *J. Met.* **43** (8) (1991) 7.
2. J. H. DEVLETIAN, S. M. DEVINCENT and S. A. GEDEON, Report MTL TR 88-47, (Army Materials Technology Laboratory, Watertown, Massachusetts, 1988).
3. E. J. LAVERNIA, J. BARAM and E. GUTIERREZ, *Mater. Sci. Eng.* **132** (1991) 119.
4. J. M. MARINKOVICH, F. A. MOHAMED, J. R. PICKENS and E. J. LAVERNIA, *J. Met.* **41** (9) (1989) 36.
5. R. W. EVANS, A. G. LEATHAM and R. G. BROOKS, *Powder Metall.* **28** (1985) 13.
6. M. GUPTA, F. A. MOHAMED and E. LAVERNIA, *Int. J. Rapid Solidifn* **6** (1991) 247.
7. E. J. LAVERNIA, *ibid.* **5** (1989) 47.
8. T. C. WILLIS, *Met. Mater.* **4** (1988) 485.
9. C. L. BUHRMASTER, D. E. CLARK and H. O. SMART, *J. Met.* **40** (1988) 44.
10. A. R. E. SINGER, *Ann. CIRP* **32** (1983) 145.
11. I. A. IBRAHIM, F. A. MOHAMED and E. J. LAVERNIA, *J. Mater. Sci.* **26** (1991) 1137.
12. A. R. E. SINGER, *Mater. Sci. Eng. A* **135** (1991) 13.
13. M. GUPTA, F. A. MOHAMED and E. J. LAVERNIA, *Metall. Trans. A* **23** (1992) 845.
14. X. LIANG, H. K. KIM, J. C. EARTHMAN and E. J. LAVERNIA, *Mater. Sci. Eng. A* **153** (1992) 646.
15. A. P. DIVECHA, S. G. FISHMAN and S. D. KUMAR, *J. Met.* **3** (9) (1981) 12.
16. S. OCHIAI and K. OSAMURA, *Metall. Trans. A* **18** (1987) 673.
17. D. L. ERICH, *Int. J. Powder Metall.* **23** (1) (1987) 45.
18. J. PAPAZIAN, *Metall. Trans. A* **19** (1988) 2845.
19. M. GUPTA, F. A. MOHAMED and E. J. LAVERNIA, *Mater. Sci. Eng. A* **144** (1991) 99.
20. V. C. NARDONE and K. W. PREWO, *Scripta Metall.* **20** (1986) 43.
21. M. HANSEN and K. ANDERKO, "Constitution of Binary Alloys" (McGraw-Hill, New York, 1958), p. 84.
22. R. E. SANDERS Jr and I. JOCELYN, US Patent 4 610 733 (1986).
23. E. GUTIERREZ, E. J. LAVERNIA, G. TRAPAGA, J. SZEKELY and N. J. GRANT, *Metall. Trans. A* **20** (1989) 71.
24. X. LIANG, J. C. EARTHMAN and E. J. LAVERNIA, *Acta Metall. Mater.* **40** (1992) 3003.
25. M. GUPTA, I. A. IBRAHIM, F. A. MOHAMED and E. J. L AVERNIA, *J. Mater. Sci.* **26** (1991) 6673.
26. M. GUPTA, F. A. MOHAMED and E. J. LAVERNIA, *Metall. Trans. A* **23** (1992) 831.
27. *Idem, J. Mater. Manuf. Proc.* **5** (2) (1990) 165.
28. J. WHITE, I. G. PALMER, I. R. HUGHES and S. A. COURT, in Proceedings, "Aluminum–Lithium Alloys V", Williamsburg, Virginia, March 1989, Vol. 3, edited by T. H. Sanders Jr and E. A. Starke Jr, p. 1635. (Materials and Components Engineering Publications, Edgbaston, UK (1989).
29. K. A. KOJIMA, R. E. LEWIS and M. J. KAUFMAN, *ibid.*, Vol. 1, p. 85.
30. R. H. BRICKNELL, *Metall. Trans. A* **17** (1986) 583.
31. X. LIANG, and E. J. LAVERNIA, *Scripta Metall.* **25** (1991) 1199.
32. E. LAVERNIA, R. H. RANGEL and T. S. SRIVATSAN, *Int. J. Atomizn Sprays* in press.
33. K. OGATA, E. J. LAVERNIA, G. RAI and N. J. GRANT, *Int. J. Rapid Solidifn* **2** (1986) 21.
34. P. BEWLAY and B. CANTOR, in "Rapidly Solidified Materials", edited by P. Lee and R. Carbonara (American Society for Metals, Metals Park, Ohio, 1986) p. 15.
35. E. J. LAVERNIA, T. ANDO and N. J. GRANT, *ibid.* p. 29.
36. V. G. MCDONNELL, E. J. LAVERNIA and G. S. SAMUELSON, in "Synthesis and Analysis in Materials Processing: Advances in Characterization and Diagnosis of Ceramic and Metal Particulate Processing", edited by E. J. Lavernia, H. Henein and I. Anderson (Metallurgical Society, Warrendale, Pennsylvania, 1989) p. 13.
37. E. J. LAVERNIA, *SAMPE Q.* **22** (2) (1991) 2.
38. Y. WU, PhD dissertation, University of California, Irvine (1991).
39. I. A. IBRAHIM, F. A. MOHAMED and E. J. LAVERNIA, in "Advanced Aluminum and Magnesium Alloys", edited by T. Khan, G. Effenberg, (ASM International, Amsterdam, 1989) p. 745.
40. L. SALVO, M. SUERY and F. DECOMPS, in "Fabrication of Particulates Reinforced Composites", edited by J. Masounave and F. G. Hamel, (ASM International, Materials Park, Ohio 1990) p. 139.
41. W. J. BOETTINGER, D. SHECHTMAN, R. J. SCHAEFER and F. S. BIANCANIELLO, *Metall. Trans. A* **15** (1984) 55.
42. H. JONES, *Phil. Mag. B* **61** (1990) 487.
43. A. F. NORMAN and P. TSAKIROPOULOS, *Int. J. Rapid Solidifn* **6** (1991) 185.
44. J. L. MURRAY, *Int. Met. Rev.* **30** (1985) 211.
45. J. A. JUAREZ ISLAS, H. JONES and W. KURZ, *Mater. Sci. Eng.* **98** (1988) 201.
46. M. RUHR, E. J. LAVERNIA and J. C. BARAM, *Metall. Trans. A* **21** (1990) 1785.
47. P. A. BECK, J. C. KREMER, L. J. DEMER and M. L. HOLZWORTH, *Trans. Met. Soc. AIME* **175** (1948) 372.
48. P. A. BECK, *J. Appl. Phys.* **19** (1948) 507.
49. P. A. BECK, J. TOWERS and W. O. MANLEY, *Trans. Met. Soc. AIME* **175** (1951) 634.
50. R. L. FULLMAN, "Metal Interfaces" (American Society for Metals, Cleveland oh, 1952) p. 179.
51. P. COTTERILL and P. R. MOULD, "Recrystallization and Grain Growth in Metals" (Surrey University Press, 1976), p. 275.
52. M. GUPTA, F. A. MOHAMED and E. J. LAVERNIA, *Metall. Trans. B* in press.
53. R. J. ARSENAULT and N. SHI, *Mater. Sci. Eng.* (1981) 175.
54. K. K. CHAWLA, A. H. ESMAEILI, A. K. DATYE and A. K. VASUDEVAN, presented at TMS/ASM Fall Meeting, Cincinnati, Ohio, October 1991.
55. H. J. RACK and R. W. KRENZER, *Metall. Trans. A* **8** (1977) 335.
56. Y. WU and E. J. LAVERNIA, *J. Met.* **43** (8) (1991) 16.
57. J. SHAKELFORD and W. ALEXANDER (eds.), "CRC Materials Science and Engineering Hand Book" (CRC Boca Raton, 1992).
58. A. R. E. SINGER and S. OZBEK, *Powder Metall.* **28** (1985) 72.
59. C. M. FRIEND, *J. Mater. Sci.* **22** (1987) 3005.
60. S. DIONNE and M. R. KRISHNADEV, in "Fabrication of Particulates Reinforced Composites", edited by J. Masounave and F. G. Hamel (ASM International, Materials Park, Ohio, 1990) p. 261.

61. M. GUPTA, C. LANE and E. J. LAVERNIA, *Scripta Metall. Mater.* **26** (1992) 825.
62. Y. FLOM and R. J. ARSENAULT, *Mater. Sci. Eng.* **77** (1986) 191.
63. A. S. ARGON and J. IM, *Metall. Trans. A* **6** (1975) 839.
64. D. L. MCDANELS, *ibid.* **16** (1985) 1105.
65. Y. WU, and E. J. LAVERNIA, *Scripta Metall. Mater.* **27** (1992) 173.
66. W. S. MILLER and F. J. HUMPHREYS, *ibid.* **25** (1991) 33.
67. W. H. HUNT Jr, J. R. BROCKENBROUGH and P. E. MAGNUSEN, *ibid.* **25** (1991) 15.
68. V. V. BHANUPRASAD, K. S. PRASAD, A. K. KURUVILLA, A. B. PANDEY, B. V. R. BHAT and Y. R. MAHAJAN, *J. Mater Sci.* **26** (1991) 460.

Received 21 July
and accepted 2 September 1992